Springer

KSME

Journal of Mechanical Science and Technology 30 (11) (2016) 5093~5101
www.springerlink.com/content/1738-494x(Print)/1976-3824(Online)
DOI 10.1007/s12206-016-1027-3

Prediction of plastic deformation under contact condition by quasi-static and dynamic simulations using explicit finite element analysis †

W. A. Siswanto[1], M. Nagentrau[1,*], A. L. Mohd Tobi[1] and M. N. Tamin[2]

[1]*Faculty of Mechanical and Manufacturing Engineering, Universiti Tun Hussein Onn Malaysia, Batu Pahat, Johor, Malaysia*
[2]*Faculty of Mechanical Engineering, Universiti Teknologi Malaysia, Johor Bahru, Johor, Malaysia*

(Manuscript Received October 29, 2015; Revised May 16, 2016; Accepted June 12, 2016)

Abstract

We compared the quasi-static and dynamic simulation responses on elastic-plastic deformation of advanced alloys using Finite element (FE) method with an explicit numerical algorithm. A geometrical model consisting of a cylinder-on-flat surface contact under a normal load and sliding motion was examined. Two aeroengine materials, Ti-6Al-4V and Super CMV (Cr-Mo-V) alloy, were employed in the FE analysis. The FE model was validated by comparative magnitudes of the FE-predicted maximum contact pressure variation along the contact half-width length with the theoretical Hertzian contact solution. Results show that the (compressive) displacement of the initial contact surface steadily increases for the quasi-static load case, but accumulates at an increasing rate to the maximum level for the dynamic loading. However, the relatively higher stiffness and yield strength of the Super CMV alloy resulted in limited deformation and low plastic strain when compared to the Ti-6Al-4V alloy. The accumulated equivalent plastic strain of the material point at the initial contact position was nearly a thousand times higher for the dynamic load case (for example, 6.592 for Ti-6Al-4V, 1.0 kN) when compared to the quasi-static loading (only 0.0072). During the loading step, the von Mises stress increased with a decreasing and increasing rate for the quasi-static and dynamic load case, respectively. A sudden increase in the stress magnitude to the respective peak value was registered due to the additional constraint to overcome the static friction of the mating surfaces during the sliding step.

Keywords: Cylinder-on-flat surface contact; Dynamic-explicit; Quasi-static; Equivalent plastic strain; Super CMV; Ti-6Al-4V

1. Introduction

Plasticity theory in contact mechanics is concerned with the distribution of plastic strains and stresses in a ductile material as the material deforms permanently when a force is applied [1]. Plastic deformation in contact mechanics is of prime importance in numerous engineering applications involving two-body contacts, such as in aeroengine and automotive engine applications. A conforming contact is defined when the surfaces of the two bodies fit closely or precisely without any deformation. The presence of any deformation at one of the contacting surfaces when there is an area of contact between the two bodies is known as a non-conforming contact [2].

It is significant to quantify the influence of the loading rate on plastic deformation of bodies with surface contact, along with plastic strain and stress distributions. A number of related studies considering both quasi-static and dynamic loading in contact mechanics in the elastic and plastic regime have been conducted [e.g., 3-7]. While quasi-static analysis is commonly found in sheet metal forming processes and collapse analysis [8], dynamic analysis is applicable to high speed machining processes [9, 10], including penetration and impact related problems [11-15].

Advanced materials such as Ti-6Al-4V and Super CMV alloys have found wide applications in gas turbines and aeroengines because of their ductility, high strength, excellent corrosion and fatigue resistance characteristics [16-20]. Local plastic deformation in contact-related problems, influenced by the loading rate in aeroengine and gas turbine applications, is a known problem. As such problem solving is costly and time consuming, finite element method has been widely employed to predict the plastic deformation associated with the contact mechanics analysis. In this respect, an appropriate numerical model must be employed to accurately reproduce the behavior of the contacting surfaces [21, 22]. Proper contact formulation should be assigned to the FE model to avoid non-convergent calculations while minimizing the simulated penetration between the mating surfaces [23, 24]. Such a complex physical problem of contact mechanics offers a challenging task, particularly for dynamic loading using the explicit FE analysis.

The strain rate-dependent mechanical response of various materials has been examined. Khan et al. [3] presented the calculated response of Ti-6Al-4V alloy under quasi-static and

*Corresponding author. Tel.: +60 17 4039241, Fax.: +60 7 4536080
E-mail address: nagentrau.rau17@yahoo.com
† Recommended by Associate Editor Heung Soo Kim

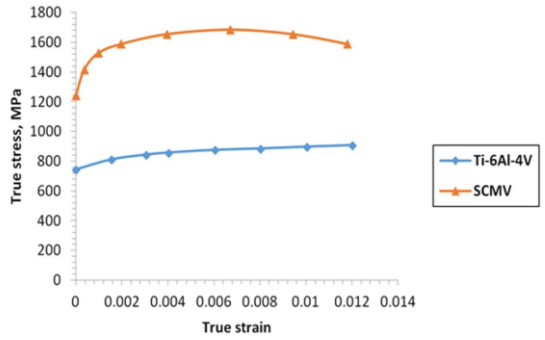

Fig. 1. Plastic stress-strain curves for Ti-6Al-4V and SCMV [25, 26].

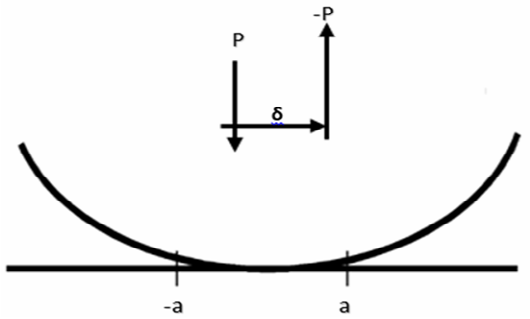

Fig. 2. Schematic view of the cylinder-on-flat contact configuration.

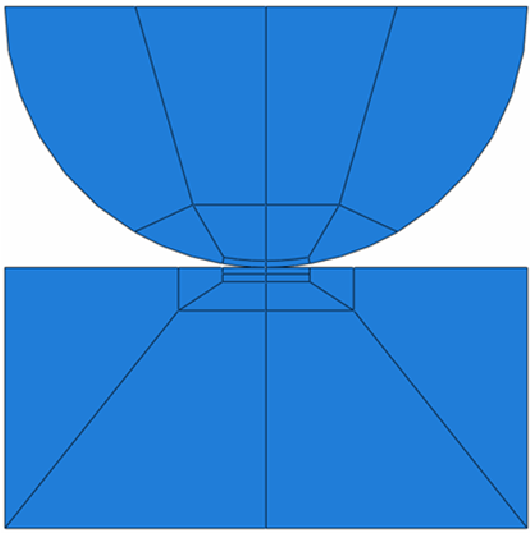

Fig. 3. Partitioned 2D geometry of the cylinder-on-flat contact for finite element mesh optimization.

dynamic loading condition, and with different temperatures. In this study, the Khan-Huang-Liang (KHL) constitutive model is compared with the established Johnson-Cook (JC) model. It is found that the KHL model better correlates the dynamic response of the alloy with measured data than with the JC model. An experimental study on the behavior of PVB laminated glass under quasi-static and dynamic loading was conducted by Xu et al. [6]. The PVB laminated glass displays a strong strain rate-dependent mechanical response under both types of loading conditions. Warhatkar et al. [5] performed tensile tests on bovine medial collateral ligaments at different applied strain rates between 0.0001 to 161/s. The results show a linear stress-strain response at lower strain rates, while non-linear behavior is established at higher strain rates. However, to the best of our knowledge, far too little attention has been paid to compare the quasi-static and dynamic simulation responses on elastic-plastic deformation of advanced alloys, including aeroengine materials such as Ti-6Al-4V and Super CMV alloys.

We compared the predicted mechanical responses of two advanced alloys under specific surface contact configuration. Both quasi-static and dynamic loading conditions were reproduced. The calculated localized plastic deformation and the associated stress fields were established using an explicit FE formulation. The theoretical solution for Hertzian contact condition serves to validate the FE model. The contact mechanics for quasi-static and dynamic loading conditions were then examined and compared.

2. Finite element simulation

2.1 Material

The materials examined in this study are titanium alloy (Ti-6Al-4V) and high-strength Cr-Mo-V steel (Super CMV), commonly used in aeroengine applications. The density, ρ of Ti-6Al-4V and Super CMV is 4.43×10^{-09} and 7.94×10^{-09} *tonne/mm*^{3}, respectively. Young's modulus, E of *115* and *200 GPa* is taken for the Ti-6Al-4V and Super CMV, respectively. Both materials assumed a Poisson's ratio, v, of *0.3* [18]. The true plastic stress-strain curves of Ti-6Al-4V [25] and Super CMV steel [26] are compared in Fig. 1. Although the initial yield strength of the super CMV of 1250 MPa is higher than that of Ti-6Al-4V, the strength retention at elevated temperature is better for the titanium alloy. In addition, it is expected that both alloys show strain-rate dependent stress-strain curves with higher values corresponding to higher strain rate loading.

2.2 Quasi-static simulation

In quasi-static simulation, a load is applied slowly such that the time rate effect such as mass inertia is negligible. The bulk material deforms under equilibrium condition. Thus, a quasi-static simulation is considered as a time-independent analysis. Fig. 2 illustrates a schematic view of the model with the cylinder-on-flat surface contact configuration. This geometrical configuration was employed in earlier experimental studies by the authors [18, 19]. The model is comprised of a half cylinder with a radius, R = 6 mm and a flat surface represented by a rectangle with 12 × 6 mm^2. The cylinder serves as the indenter on the flat surface. The corresponding 2D view of the model, as shown in Fig. 3, was used as the FE model in this study. Quasi-static simulation was performed using the ABAQUS explicit algorithm (version *6.13)*. The explicit analysis was chosen to maintain identical numerical solution method with that of the dynamic analysis, for comparative purposes. The

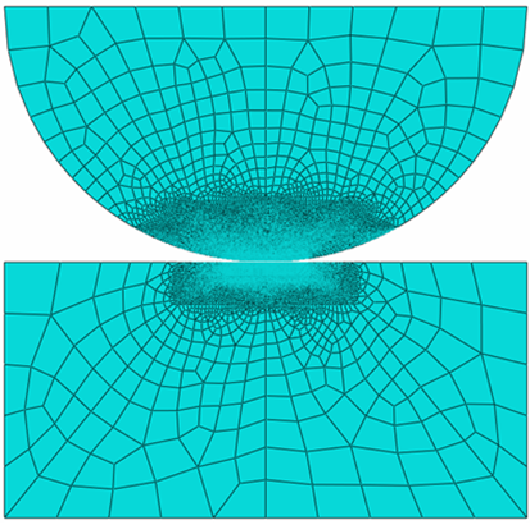

Fig. 4. Mesh module of the 2D cylinder-on-flat surface contact model.

equilibrium condition was ensured by maintaining the minimum (practically zero) kinetic energy term following the convergence process. The FE model was discretized into linear quadrilateral plane strain elements. The bottom surface of the model was constrained in all displacement directions and rotations. The penalty contact algorithm with the friction coefficient, $\mu = 0.3$ was assumed for all surfaces in contact.

In view of the expected high gradient of the calculated variables (equivalent plastic strain and von Mises stress) in the vicinity of the contact region, the region was discretized into smaller size elements. The element mesh transition from coarse-to-fine was achieved via a controlled edge seeding technique. The resulting element mesh density is illustrated in Fig. 4 with elements in the contact region having an edge length of 5 μm. Such element size ensures that the FE-calculated results are independent of the size of the elements.

The loading was simulated in three steps. The first step is the application of the concentrated normal force to the cylindrical indenter. The load is ramped at a prescribed constant speed. An equation-type constraint was used to ensure the top surface of the indenter half-model moves simultaneously with the point load. Once the maximum prescribed load magnitude is achieved, the indenter is dragged over a distance of 0.1 mm to simulate the sliding of the indenter across the flat surface. The final step consists of unloading of the indenter. The maximum applied force to the indenter and the corresponding loading rate for the validation and load cases are listed in Table 1. The relatively slow loading rates represent the quasi-static loading conditions. The contact pressure distribution and contact half-width length of the quasi-static model was validated with the theoretical Hertzian contact solution.

2.3 Dynamic-explicit simulation

The FE simulation of the dynamic load cases was performed using the explicit algorithm. In the dynamic simulation, the applied load to the model is prescribed over a relatively short time period. Inertia and induced vibration effects on the structure are accounted for in the analysis. The loading rates for the dynamic-explicit simulation are listed in Table 2. The total time prescribed for the three steps of the dynamic-explicit analysis is 8.10×10^{-07} *s*.

Other parameters of the FE model used for the dynamic-explicit analysis are identical to those employed in the quasi-static simulation cases. These include the contact configuration, type of plane strain elements, element mesh densities, boundary conditions and the sliding displacement. In this manner, the predicted mechanics of the indenter-on-flat surface contact could be evaluated based on the quasi-static and dynamic response of each material system. The indenter-on-flat surface contact condition was also prescribed with identical penalty contact algorithm using the friction coefficient, $\mu = 0.3$ as in the quasi-static simulation. However, the friction coefficient value, μ is likely to reduce in the dynamic (kinetic friction) condition.

Table 1. Loading conditions for quasi-static analysis.

Case	Max load (kN)	Loading rate (kN/s)
Validation	0.50	3.33×10^3
Load 1A	0.75	5.00×10^3
Load 1B	1.00	6.67×10^3

Table 2. Loading conditions for dynamic analysis.

Case	Max load (kN)	Loading rate (kN/s)
Validation	0.50	617.28×10^3
Load 2A	0.75	925.93×10^3
Load 2B	1.00	1234.57×10^3

3. Results and discussion

The FE-predicted deformation responses of the indenter-on-flat surface made of Ti-6Al-4V and Super CMV alloy under quasi-static and dynamic loading conditions were compared. The FE simulations of the contact mechanics were performed using the explicit algorithm. The FE model was validated against theoretical Hertzian contact solution for the contact pressure and the contact half-width length. Results are presented in terms of the evolution characteristics of the equivalent plastic strains, von Mises stresses and internal kinetic energy terms.

3.1 Finite element model validation

The FE model of the indenter-on-flat surface contact was validated based on the variation of the contact pressure along the contact half-width length. The FE-predicted variations of the contact pressure and half-width length are comparable to that of the analytical Hertzian contact solution for the quasi-static loading case, as shown in Fig. 5 for Ti-6Al-4V alloy.

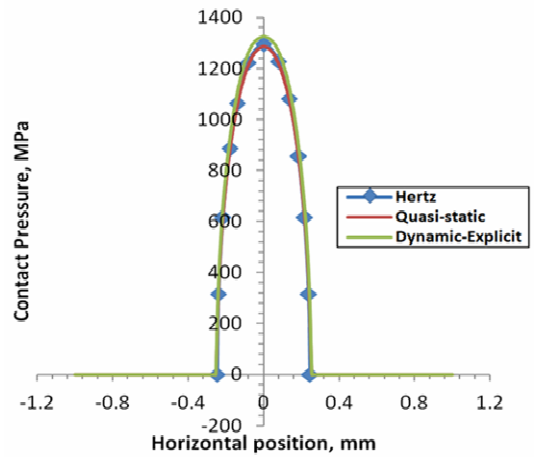

Fig. 5. Contact pressure and contact half-width length comparison between quasi-static, dynamic-explicit simulations and Hertzian contact theoretical solution for Ti-6Al-4V.

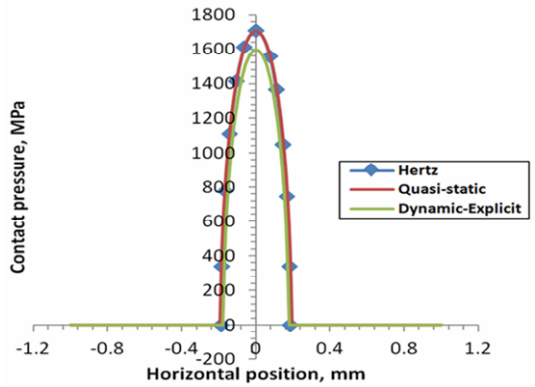

Fig. 6. Contact pressure and contact half-width length comparison between quasi-static, dynamic-explicit simulations and Hertzian contact theoretical solution for Super CMV.

The peak contact pressure of p_0 =1286.24 and 1294.64 MPa, is predicted through the quasi-static FE simulation and Hertzian contact solution, respectively. The peak pressure developed at the initial line of contact between the indenter and the flat surface, in the center of the contact region. The corresponding FE-predicted contact half-width length, a at 0.26 mm for both quasi-static and dynamic load cases is comparable to that calculated using Hertzian solution at 0.25 mm. These comparable FE-predicted magnitudes of the contact pressure and contact half-width-length with the theoretical Hertzian solution serve to validate the explicit FE model. Results also show that a higher peak contact pressure at 1325.61 MPa is predicted for the dynamic loading.

Similar quality of the FE model prediction is demonstrated for Super CMV alloy as shown in Fig. 6. The maximum contact pressure, p_0 for quasi-static loading case is similar at 1704.54 and 1707.32 MPa for the FE-predicted and theoretical Hertzian solution, respectively. The corresponding contact half-width length, a for quasi-static and dynamic simulation cases is 0.19 and 0.20 mm, respectively.

Table 3. Comparisons of contact variables for the two alloys examined.

Material	Ti-6Al-4V	Super CMV
Maximum contact pressure, MPa (Hertzian solution)	1294.64	1707.32
Maximum contact pressure, MPa (Quasi-static)	1286.24	1704.54
% error	0.65	0.16
Maximum contact pressure, MPa (Dynamic-explicit)	1325.61	1597.51
% error	2.39	6.43
Contact half-width length, mm (Hertzian solution)	0.25	0.19
Contact half-width length, mm (Quasi-static)	0.26	0.20
% error	4.00	5.26
Contact half-width length, mm (Dynamic-explicit)	0.26	0.18
% error	4.00	5.26

Table 3 compares the critical contact parameter values for the two ductile alloys as predicted by explicit FE analyses and the theoretical Hertzian contact solution. The slight difference is due to the elastic half-space assumption employed in the theoretical Hertzian contact solution. Higher peak contact pressure predicted for Super CMV is derived from the higher hardening curve of the material compared to that of Ti-6Al-4V alloy. Since the strain-rate dependent stress-strain curve of the material is not prescribed, the apparently lower contact pressure response of the Super CMV alloy predicted for the dynamic load case is associated with the mass inertia effect only. Identical penalty contact algorithm employed in both quasi-static and dynamic load cases resulted in similar predicted contact half-width lengths.

3.2 History of deformation

The deformation response of the indenter-on-flat surface contact system throughout the loading steps is represented by the displacement history of the substrate for the initial material point lying underneath the indenter. The evolution of the vertical (compressive) displacements for the quasi-static and dynamic loading case is shown in Figs. 7 and 8, respectively. In quasi-static loading case, the displacement steadily increases to the maximum level as the peak applied load is reached. The higher magnitude of the displacement at peak load is registered for the relatively lower stiffness Ti-6Al-4V alloy (13.84×10^{-3} and 18.18×10^{-3} mm for the peak load of 0.7 and 1.0 kN, respectively) when compared to Super CMV alloy (8.50×10^{-3} and 10.90×10^{-3} mm). The load level is maintained throughout the subsequent sliding step. The amount of elastic recovery following the unloading step depends on the amount of subsurface plastic strain induced during the sliding step (refer also to Figs. 9 and 10).

The explicit FE-predicted dynamic response shows a con-

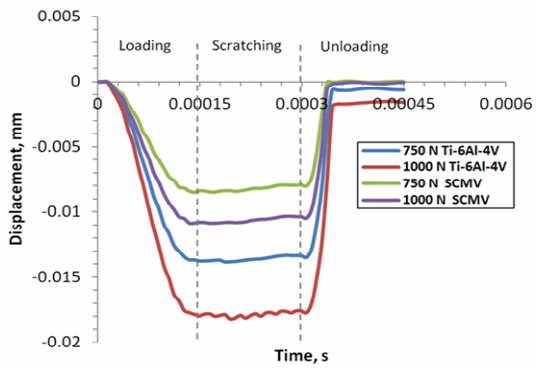

Fig. 7. The displacement history of the initial contact point in the substrate for quasi-static simulation.

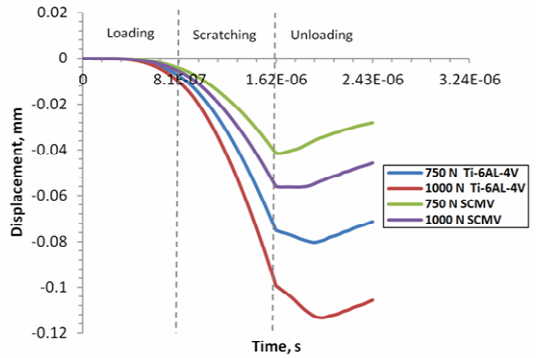

Fig. 8. The displacement history of the initial contact point in the substrate for the dynamic simulation.

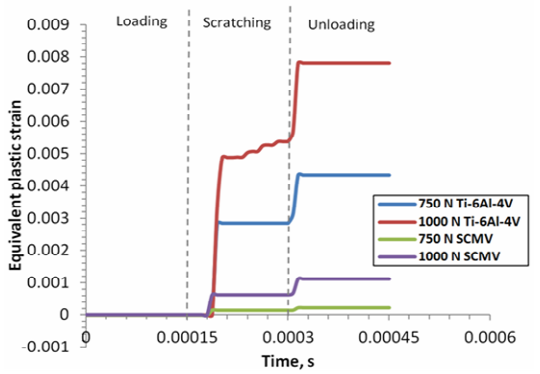

Fig. 9. The equivalent plastic strain history of the initial contact point in the substrate for quasi-static simulation.

tinuous non-linear increase in the compressive displacement of the substrate throughout the loading and sliding steps. This localized deformation occurs at an increasing displacement rate. In fact, the inertia (dynamic) effect of the moving indenter mass causes the maximum displacement level at the initial contact point to be reached during the unloading stage for Ti-6Al-4V alloy (80.39×10^{-3} and 113.27×10^{-3} mm for the peak load of 0.7 and 1.0 kN, respectively). The harder and stiffer Super CMV material did not exhibit such unloading response. In addition, the predicted dynamic response also shows a higher maximum substrate deformation reached at

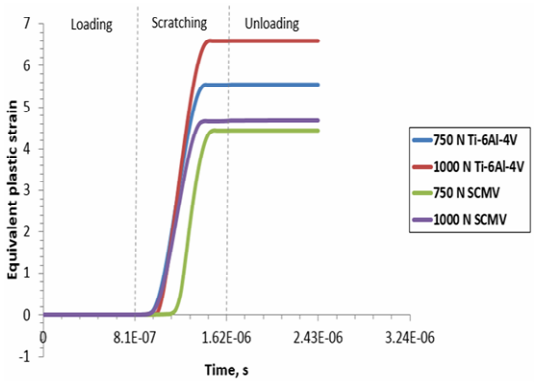

Fig. 10. The equivalent plastic strain history of the initial contact point in the substrate for dynamic-explicit simulation.

each respective peak load when compared to the quasi-static loading cases. The non-zero displacement recorded at the end of the unloading stage is a consequence of the plasticity-induced deformation, as described in the next section.

3.3 Evolution of the equivalent plastic strain

Plastic deformation in the substrate of the indenter-on-flat surface contact system is represented in terms of the equivalent plastic strain. The FE-predicted evolution of the equivalent plastic strain for the quasi-static and dynamic loading step is shown in Figs. 9 and 10, respectively. In both loading cases, the loading step corresponds to elastic behavior only. Plasticity initiates and is practically maintained during the sliding step (except for Ti-6Al-4V alloy for the maximum applied load of 1.0 kN). The additional plastic strain increment is predicted at the end of the sliding step due to the highly constrained plastic deformation at the current point of contact. The accumulated equivalent plastic strain in the Ti-6Al-4V alloy, at the initial point of contact is 0.434 and 0.782 %, corresponding to the applied peak load of 0.75 and 1.0 kN, respectively. Much lower level of the accumulated plastic strain is predicted for the harder Super CMV material at 0.112 and 0.024 %, respectively. This is due to the higher subsequent yield strengths for the strain-hardening material [18, 28].

The equivalent plastic strain at the initial contact point in the substrate continuously increases to the respective maximum level during the sliding step for the dynamic load cases. Much higher plastic strain is accumulated when compared to the quasi-static load case. For example, the accumulated equivalent plastic strain of 6.592 is predicted for the Ti-6Al-4V alloy corresponding to the applied load of 1.0 kN (0.00782 for the quasi-static case); a nearly thousand times higher. The plastic strain level is maintained throughout the subsequent unloading step as this step is associated with elastic response only.

3.4 Evolution of von Mises stress

The evolution of the corresponding von Mises stress at the initial contact point in the substrate throughout the loading

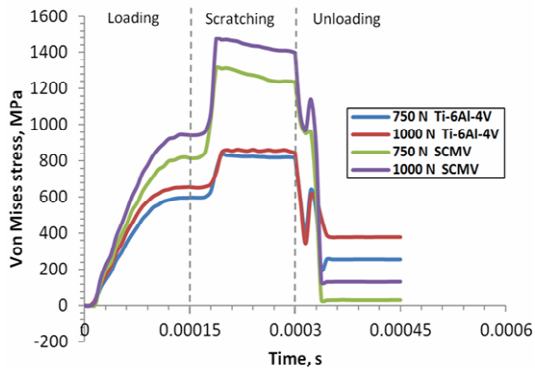

Fig. 11. The von Mises stress history of the initial contact point in the substrate for quasi-static simulation.

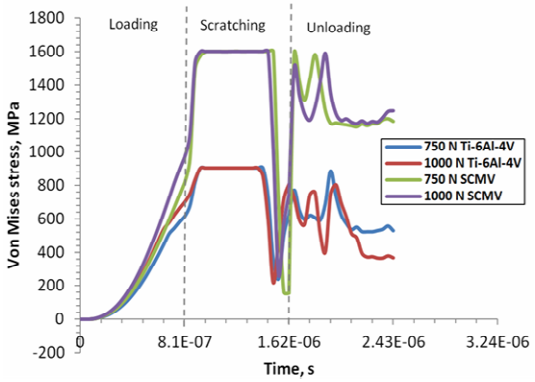

Fig. 12. The von Mises stress history of the initial contact point in the substrate for the dynamic-explicit simulation.

steps is shown in Figs. 11 and 12, respectively, for the quasi-static and dynamic load cases. In the quasi-static load case, the stress steadily increases during the loading step to reach the yield strength level in each respective material. A sudden increase in the stress magnitude to a peak of 834.24 and 863.69 MPa for the applied load case of 0.75 and 1.0 kN, respectively in Ti-6Al-4V alloy is registered due to the additional constraint to overcome the static friction of the mating surfaces. Such increase in stress corresponds to the induced plastic strain in the hardening material. Although the plastic strain induced during the sliding step is higher, the von Mises stress magnitude is lower in Ti-6Al-4V compared to that in the Super CMV alloy. The maximum von Mises stress reaches 1.31 and 1.47 GPa for the applied load case of 0.75 and 1.0 kN, respectively, in the Super CMV alloy. Such response is dictated by the hardening characteristic of each material, with relatively limited hardening of Ti-6Al-4V alloy as depicted in Fig. 1. The material point maintains some residual stress following complete unloading, primarily due to the constrained plastic deformation by the surrounding bulk elastic substrate.

In the dynamic loading condition, the von Mises stress evolves at an increasing rate. Additional stress reaches a peak in overcoming the friction. The identical maximum stress level is maintained by each material at the peak applied load (0.90 GPa and 1.60 GPa, for Super CMV and Ti-6Al-4V alloy,

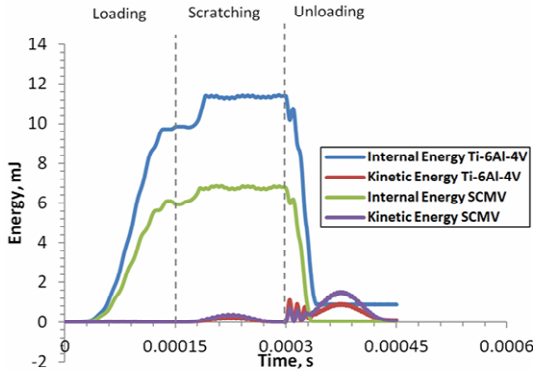

Fig. 13. The evolution of internal and kinetic energy of the indenter-on-flat surface contact system for quasi-static simulation.

respectively) during the sliding step. The higher maximum stress level reached for the dynamic load case reflects the significance of the strain-rate effect on the materials response. At the end of the sliding step, the indenter, thus the contacting surfaces, has displaced away from the initial contact position. Consequently, the material point at the initial contact experiences an earlier unloading effect, manifested by the sudden load drop as shown in Fig. 12. The observed 'dip" in the calculated von Mises stress during unloading is caused by the change in the numerical sign of some Cartesian stress components [29]. The higher residual stress level is predicted for the dynamic load case relative to the quasi-static condition. In view of the relatively high plastic strain rate experienced by the material, the magnitude of the residual plastic strains and stresses could be accurately assessed by considering the strain rate-dependent stress-strain curves of the materials in the FE simulation. The evolutionary trends and relative magnitudes of the calculated variables, however, are expected to remain similar. Thus, the quantitative description of the mechanics of materials for the cylindrical indenter-on-flat surface contact as deliberated in this paper is appropriate.

3.5 Evolution of internal energy terms

The different energy terms are calculated during the deformation of the substrate in the indenter-on-flat surface contact system. The internal energy term represents the sum of the recoverable elastic strain energy and dissipated energy by plasticity and viscoplasticity. The kinetic energy term is associated with the mass and its velocity. The evolution of both internal and kinetic energies for the entire indenter-on-flat surface contact system is shown in Figs. 13 and 14 for the quasi-static and dynamic load cases, respectively.

The kinetic energy associated with any static or quasi-static system should be zero or at its minimum. The calculated non-zero magnitude of the kinetic energy term for a quasi-static system is caused by the explicit numerical scheme during the iterations to equilibrium. Force equilibrium is considered when an iteration converged with practically zero calculated kinetic energy term as shown in Fig. 13 for quasi-static load

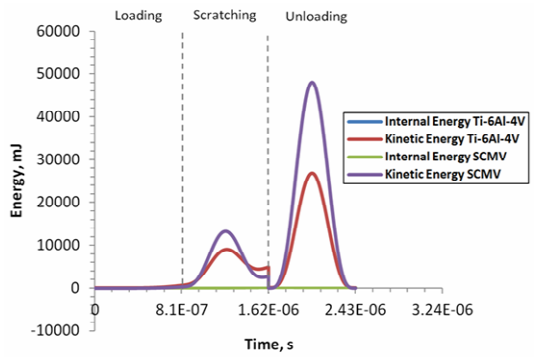

Fig. 14. The evolution of internal and kinetic energy of the indenter-on-flat surface contact system for dynamic simulation.

case. The calculated kinetic energy term should remain below 5 % of the total internal energy of the system for a quasi-static deformation process [8]. The internal energy evolves to a higher level in Ti-6Al-4V alloy than that in Super CMV alloy in view of the high strength and hardening of the latter. The energy is almost fully recovered by the Super CMV alloy following the unloading step, indicating the insignificant plastic dissipation energy (also reflected in the minute amount of the induced plastic strain, see Fig. 9). The residual elastic energy stored in Ti-6Al-4V alloy at the end of the unloading step is due to the constrained elastic deformation surrounding the localized plastic region.

Contrary to the quasi-static load case, the kinetic internal energy for the dynamic loading is significant as contributed by both the mass inertia and velocity effects. The first calculated peak of the kinetic energy term is associated with the movement of the indenter in compressing the deforming flat surface. The occurrence of the peak energy is delayed due to the inertia effect. The second and higher peak are associated with the sliding process, and the delay is due to the elapsed time for the indenter to reach the peak at the new position, while the calculated evolution is monitored at the initial contact position. The internal energy associated with the localized deformation of the contact region is relatively very small (0.19 and 0.31 kJ) compared to the kinetic energy of the system (48 and 26 kJ for Super CMV and Ti-6Al-4V alloys, respectively) for the applied load of 1.0 kN. Thus the inclusion of the internal energy in the Fig. 14 would not visually alter the plot, for the given scale used.

4. Conclusions

We compared the predicted response of circular indenter-on-flat surface contact system for Ti-6Al-4V and Super CMV alloy under quasi-static and dynamic load cases. The explicit FE model was validated using the theoretical Hertzian contact solution for the maximum contact pressure and contact half-width length. In the absence of the strain rate-dependent stress-strain curves of the materials for the FE simulations, the dynamic response was derived only from the mass inertia effect. Results show that:

- The higher magnitude of the contact pressure developed in the Super CMV alloy is attributed to the higher strength of the material compared to Ti-6Al-4V alloy. However, the use of identical penalty contact algorithm and coefficient of friction value resulted in similar contact half-width length for both quasi-static and dynamic load cases.
- The (compressive) displacement of the initial contact surface steadily increases for the quasi-static load case, while accumulating at an increasing rate to the maximum level for the dynamic load case.
- The accumulated equivalent plastic strain of the material point at the initial contact position is nearly a thousand times higher for the dynamic load case (for example, 6.592 for Ti-6Al-4V, 1.0 kN) when compared to the quasi-static loading (only 0.0072). A continuous increase in the strain is predicted for the dynamic load case.
- During the loading step, the von Mises stress increases with a decreasing and increasing rate for the quasi-static and dynamic loading case, respectively. A sudden increase in the stress magnitude to the respective peak value is registered due to the additional constraint to overcome the frictional effect of the mating surfaces during the sliding step.

The practical application of the presented results for the cylinder-on-flat contact configuration is found in evaluating the contact conditions in numerous aeroengine components. The specific materials are Ti-6Al-4V and Super CMV alloys. The results are also applicable in assessment of potential damage associated with plastic deformation under quasi-static and dynamic load cases. Such application is targeted to improve performance and reducing maintenance cost of gas turbine transmission components such as spline couplings, via proper material selection.

Acknowledgments

The authors acknowledge the financial support by the Ministry of Education Malaysia, Universiti Tun Hussein Onn Malaysia (UTHM) and Universiti Teknologi Malaysia (UTM) through Research Acculturation Collaborative Effort (RACE) grant No. 1441(UTHM) and No. 00M26 (UTM).

Nomenclature

E	: Elastic modulus
v	: Poisson ratio
δ	: Displacement
P	: Force
μ	: Friction coefficient
a	: Contact half-width length
po	: Maximum contact pressure
R	: Radius

ρ : Density

References

[1] J. Chakrabarty, *Theory of plasticity,* Butterworth-Heinemann (2012).

[2] K. L. Johnson, *Contact mechanics,* Cambridge University Press (1987).

[3] A. S. Khan, Y. S. Suh and R. Kazmi, Quasi-static and dynamic loading responses and constitutive modeling of titanium alloys, *International J. of Plasticity*, 20 (12) (2004) 2233-2248.

[4] A. S. Khan, M. Baig, S. H. Choi, H. S. Yang and X. Sun, Quasi-static and dynamic responses of advanced high strength steels: experiments and modeling, *International J. of Plasticity*, 30 (2012) 1-17.

[5] H. Warhatkar, A. Chawla, S. Mukherjee and R. Malhotra, *Experimental Study of Variation between Quasi-static and Dynamic Load Deformation Properties of Bovine Medial Collateral Ligaments,* No. 2009-01-0392, SAE Technical Paper (2009).

[6] J. Xu, Y. Li, B. Liu, M. Zhu and D. Ge, Experimental study on mechanical behavior of PVB laminated glass under quasi-static and dynamic loadings, *Composites Part B: Engineering*, 42 (2) (2011) 302-308.

[7] O. S. Hopperstad, T. Børvik, M. Fourmeau, K. O. Pedersen and A. Benallal, Quasi-static and Dynamic Fracture of High-strength Aluminium Alloy, *Procedia Materials Science*, 3 (2014) 51-56.

[8] Dassault Systemes, *Abaqus Theory Manual. Version 6.13. RI*, USA (2013).

[9] A. Molinari, C. Musquar and G. Sutter, Adiabatic shear banding in high speed machining of Ti-6Al-4V: experiments and modeling, *International J. of Plasticity,* 18 (4) (2002) 443-459.

[10] T. J. Burns and M. A. Davies, On repeated adaiabatic shear band formation during high speed machining, *International J. of Plasticity,* 18 (4) (2002) 487-506.

[11] A. Gilat and C. S. Cheng, Modeling torsional split Hopkinson bar tests at strain rates above 10,000 per sec, *International Journal of Plasticity,* 18 (5-6) (2002) 787-799.

[12] A. S. Khan and O. Lopez-Pamies, Time and temperature-dependent response and relaxation of a soft polymer, *International J. of Plasticity*, 18 (10) (2002) 1359-1372.

[13] A. S. Khan, O. U. Colak and P. Centala, Compressive failure strengths and modes of woven S2-glass reinforced polyester due to quasi-static and dynamic loading, *International J. of Plasticity,* 18 (10) (2002) 1337-1357.

[14] T. Bjerke, Z. Li and J. Lambros, Role of plasticity in heat generation during high rate deformation and fracture of polycarbonates, *International J. of Plasticity*, 18 (4) (2002) 549-567.

[15] S. Yao, L. Sun and X. Ma, Quasi-static compression of electric resistance welded mild steel tubes with axial gradient-distributed microstructures, *J. of Mechanical Science and Technology*, 30 (5) (2016) 1957-1965.

[16] T. Ford, Main shafts for the Trent, *Aircraft Engineering and Aerospace Technology*, 69 (6) (1997) 555-560.

[17] T. R. Hyde, *Development of a representative specimen for fretting fatigue of spline joint couplings,* Nottingham: University of Nottingham (2002).

[18] A. L. Mohd Tobi, J. Ding, G. Bandak, S. B. Leen and P. H. Shipway, A study on the interaction between fretting wear and cyclic plasticity for Ti-6Al-4V, *Wear,* 267 (1) (2009) 270-282.

[19] I. R. McColl, J. Ding and S. B. Leen, Finite element simulation and experimental validation of fretting wear, *Wear,* 256 (11) (2004) 1114-1127.

[20] J. Elanchezhian, M. P. Kumar and G. Manimaran, Grinding titanium Ti-6Al-4V alloy with electroplated cubic boron nitride wheel under cryogenic cooling, *J. of Mechanical Science and Technology*, 29 (11) (2015) 4885-4890.

[21] V. Ciampi and M. A. Crisfield, Non-linear finite element analysis of solids and structures, *Meccanica*, 32 (6) (1997) 586-587.

[22] E. A. De Souza Neto, D. Peric and D. R. Owen, *Computational methods for plasticity: theory and applications,* Wiley (2011).

[23] P. Wriggers and G. Zavarise, *Computational contact mechanics*, Encyclopedia of computational mechanics (2004).

[24] T. A. Laursen, *Computational contact and impact mechanics: fundamentals of modeling interfacial phenomena in nonlinear finite element analysis*, Springer Science and Business Media (2002).

[25] M. Benedetti and V. Fontanari, The effect of bi-modal and lamellar microstructures of Ti-6Al-4V on the behaviour of fatigue cracks emanating from edge-notches, *Fatigue and Fracture of Engineering Materials and Structures*, 27 (11) (2004) 1073-1089.

[26] S. B. Leen, I. J. Richardson, I. R. McColl, E. J. Williams and T. R. Hyde, Macroscopic fretting variables in a splined coupling under combined torque and axial load, *J. of Strain Analysis for Engineering Design*, 36 (5) (2001) 481-497.

[27] M. Nagentrau, W. A. Siswanto and A. L. Mohd Tobi, Investigation on the effect of linear kinematic hardening model on plasticity prediction of reciprocating sliding contact, *Applied Mechanics and Materials*, 773-774 (2015) 183-187.

[28] R. Li, T. H. Hyde and W. Sun, Finite element prediction of fatigue crack growth in Super CMV hollow shafts with transverse holes under combined torsional and axial loading, *J. of Strain Analysis for Engineering Design*, 48 (7) (2013) 457-469.

[29] P. A. Allen and C. D. Wilson, Hydrostatic stress effect on the yield behavior of inconel 100, *J. of the Mechanical Behavior of Materials*, 15 (1-2) (2004) 27-48.

Waluyo Adi Siswanto is an Associate Professor in Faculty of Mechanical and Manufacturing Engineering, Universiti Tun Hussein Onn Malaysia (UTHM). His research interests are in the finite element analysis and computational mechanics.

Nagentrau Muniandy is a Research Assistant in Faculty of Mechanical and Manufacturing Engineering, Universiti Tun Hussein Onn Malaysia (UTHM). His research interests are in finite element analysis for contact problems and plastic deformation.

Abdul Latif Mohd Tobi is a Senior Lecturer in Faculty of Mechanical and Manufacturing Engineering, Universiti Tun Hussein Onn Malaysia (UTHM). His research interests are in coating fracture and wear modelling.

Mohd Nasir Tamin is a Professor in the Faculty of Mechanical Engineering, Universiti Teknologi Malaysia (UTM). His research interests are in fatigue and fracture mechanics, and computational solid mechanics.